Forecasting **Products**

Research and Development

Forecasting Research
Technical Report No. 267

Freezing fog and the implications for airline de-icing practice at UK airports

by

R. Brown

May 1999

The Met.Office

Excelling *in weather services*

Forecasting Research
Technical Report No. 267

Freezing fog and the implications for airline de-icing practice at UK airports

by

R. Brown

May 1999

Meteorological Office
F Division
Room R325
London Road
Bracknell
Berkshire
RG12 2SZ
United Kingdom

Tel 44 (0) 1344 854937 e-mail: jsarmstrong@meto.gov.uk

Contents

1. Introduction

When freezing fog is reported aircraft are only allowed to take off, if at all, after a full ground de-icing. This restriction may be unnecessarily strict, following a change in the definition of freezing fog from ice being deposited, to visibility less than 1000 m and temperature below 0°C. This study therefore concerns the estimation of supercooled fog liquid water content from visibility and also the frequency of occurrence of supercooled fog in different visibility bands below 1000 m. The problem arises from a change in the reporting practice for the METAR code for freezing fog used at airfields. This now differs from the reporting practice for the SYNOP code used at other meteorological stations. The instructions for reporting freezing fog are as follows -

SYNOP: Fog depositing rime (If no rime choose another fog code).

METAR: WMO Manual of Codes Para. 15.8.9 Note 1: 'Any fog consisting predominantly of water droplets at temperatures below 0°C *shall* be reported as freezing fog (FZFG), *whether it is depositing rime or not'*.

Airline practice has been to de-ice aircraft before take off when freezing fog is reported according to the METAR code. This is because the METAR code originally only required freezing fog to be reported when fog was depositing rime, as does the SYNOP code. With the change to the METAR code, it is believed that aircraft are being de-iced unnecessarily, because freezing fog with visibility approaching 1000 m is likely to have an insignificant liquid water content (LWC). If the restriction could be relaxed, possibly with the aid of instrumentation to measure fog LWC or drop size, the number of wasted ground de-icings could be reduced.

The key problem in estimating fog LWC from visibility is that there is not a one to one correspondence between them. The visibility depends both on the LWC and the size distribution of the fog drops. Fogs comprising small drops have a lower visibility for a given LWC than fogs comprising large drops. This aspect is considered in detail because drop size information is not available operationally. The study examines the relationship between LWC and visibility using theoretical relationships and published experimental data. The results are used in conjunction with freezing fog statistics obtained from Heathrow and Gatwick to obtain a provisional estimate of the number of occasions per year when de-icing could be avoided when freezing fog is reported in the METAR code. Uncertainty in the estimate arises from ambiguities in the observations, the lack of information on the thickness of accreted ice constituting a hazard and also from the uncertainty in the capture efficiency of fog drops at low airspeeds. Finally, the possibility of real-time measurements of LWC or drop size is considered.

2. A Basic Guide to Freezing Fog

In order to help the reader understand the issues involved in relating visibility and liquid water content, a brief guide to some fundamental aspects of freezing fog is provided first. When the air becomes saturated due to cooling, water vapour condenses on small particles called nuclei. It will not spontaneously condense on nothing under normal atmospheric conditions. The vast majority of nuclei produce water drops even at temperatures below 0°C and these are known as cloud condensation nuclei (CCN). In fact, it is possible to cool pure water drops floating in air down to -40°C before they freeze spontaneously. A few nuclei produce ice crystal and these are known as ice nuclei. Their concentration increases dramatically at temperatures well below 0°C. However, for temperatures typical of freezing fog in this country, the concentration of ice nuclei is generally negligible, so the fogs comprise supercooled liquid water drops. If a significant concentration of ice crystals does

develop in a fog, they will grow much faster than the water drops and eventually cause the drops to evaporate (as in essence water vapour is transferred from the drops to the ice crystals). As the ice crystals grow they develop a significant fall speed and are deposited on the ground. The visibility rises significantly when this happens. The author has seen evidence of this behaviour in one or two freezing fogs in Bracknell, possibly due to a local source of ice nuclei. It can be assumed therefore that in the UK dense freezing fogs are comprised primarily of supercooled water drops.

The behaviour of CCN is also important in understanding the relationship between visibility and LWC. As the relative humidity increases on a clear night due to cooling, but before the air becomes saturated, the CCN swell as they absorb water to form very small droplets. The size each CCN grows to depends upon its mass and the ambient relative humidity. As cooling continues and the air becomes supersaturated (i.e. relative humidity exceeds 100 %) condensation occurs leading to a dense fog. From the CCN perspective, once the air becomes supersaturated the sizes of the largest CCN are no longer constrained by the relative humidity (which exceeds 100%). They start to grow rapidly into fog drops and are said to be activated. The smaller CCN are not activated, which means their size is still tied to the prevailing relative humidity and they remain much smaller than fog drops. The unactivated drops in a fog are often referred to as haze droplets. Droplets with radius less than around 2 μm (1 μm = 1 millionth of a metre) can be considered haze droplets. A complicating factor, discussed in detail in Appendix B, is that the haze droplets can be responsible for a reduction in visibility whilst making an insignificant contribution to the fog liquid water content.

3. Analysis of Observations of Freezing Fog

In order to determine the scope of the problem, an analysis has been made of synoptic observations made at Heathrow, Gatwick and Manchester Airports.

3.1 Hourly Observations

Hourly observations from Heathrow have been analysed for the twenty-year period 1 January 1977 - 31 December 1996. This should be a late enough period to avoid pollution events atypical of conditions now. The total number of hourly observations from Heathrow was 175320, of which 5491 (3.13%) were below 0°C. Of the sub-zero observations, 539 (9.8%) had a visibility less than 1000 m.

By comparing the hourly temperature and visibility (V) observations with the reported weather type in the SYNOP code (i.e. fog depositing rime or fog not depositing rime), an analysis of the occurrence of reported rime deposition has been performed. Of the 539 observations with $T < 0°C$ and $V < 1000$ m, 234 (43.4%) reported rime deposition and 305 (56.6%) reported fog not depositing rime. The average number of hours per year with rime deposition was 11.7.

It was hoped to establish from the analysis that rime deposition was confined to low visibilities, implying higher LWC values as indicated in Tables 3 and 4 in Section 4. This was found to be substantially, but not entirely, true. The temperature depression below 0°C was found also to be a factor. The percentage of occasions with rime deposition when $V < 1000$ m has been examined as both a function of visibility and temperature. The essential features of the results are shown in Tables 1 and 2. It can be seen from Table 1 that for $V < 200$ m rime deposition is reported on 65% of occasions, whilst Table 2 shows that for $V > 200$ m rime deposition is reported on only 23 % of occasions. Similar results to a 200 m threshold are obtained for $V < 100$ m, Table 1. Also, similar results to a 200 m threshold are obtained for $V > 300$ m, Table 2 and for higher visibility thresholds. Therefore, 200 m seems to be a significant threshold for rime deposition. It was not anticipated that on up to 38% of occasions with $V < 200$ m or $V < 100$ m no rime deposition would be reported. Table 1 shows that this feature is temperature dependent. If the temperature is between 0 and -1°C

only 34 - 38 % of fogs are reported as depositing rime for V < 200m or V < 100 m, but this rises to 84% if T < -3°C.

Table 1 Distribution of Riming and Non Riming Observations Below Two Visibility Thresholds

	V < 100 m			**V < 200 m**		
T (°C)	Rime	No Rime	% Rime	Rime	No Rime	% Rime
< -3.	**36**	**7**	**84**	**48**	**9**	**84**
-3 to -2.1	**18**	**8**	**69**	**55**	**13**	**81**
-2 to -1.1	**23**	**12**	**66**	**65**	**27**	**71**
-1 to -0.1	**15**	**29**	**34**	**38**	**61**	**38**
Total	**92**	**56**	**62**	**206**	**110**	**65**

Table 2 Distribution of Riming and Non Riming Observations Above Two Visibility Thresholds

	200 < V < 1000 m			**300 < V < 1000 m**		
T (°C)	Rime	No Rime	% Rime	Rime	No Rime	% Rime
< -3	**10**	**30**	**25**	**9**	**27**	**25**
-3 to -2.1	**6**	**46**	**12**	**4**	**37**	**11**
-2 to -1.1	**26**	**43**	**38**	**21**	**37**	**36**
-1 to -0.1	**18**	**74**	**20**	**14**	**55**	**20**
Total	**60**	**193**	**23**	**48**	**156**	**24**

The temperature dependence may be due to the release of latent heat upon freezing. This has to be removed from the droplet to allow freezing to be completed. It has to be lost either to the air or to the object upon which condensation is occurring. The latent heat will be removed more quickly if the object is well below zero. The physics is essentially that leading to rime ice at low temperatures but glazed ice nearer to 0°C during aircraft icing.

The small but not insignificant number of reports of no rime deposition with V < 200 m or < 100 m and T < -3°C are not easily explained. The simplest explanation is to assume observer error in making what must be a difficult observation, especially at night. Since it appears that one cannot always rely on the synoptic observation to determine if riming is occurring, this is possibly one reason for the change to the METAR code.

There are also 20% of occasions when rime deposition was reported and the visibility was above 500 m. Section 4 shows that very low liquid water contents should be present. To explain this one can again appeal to the difficulty of making the observation of rime deposition. For example, if the temperature was initially above 0°C and surfaces were wetted by dew deposition, this could eventually freeze if the temperature fell below zero. How would the observer distinguish this from rime deposition. An analysis of the individual observations shows that on 50% of occasions when the visibility was greater than 300 m and rime deposition was reported, the visibility had been less than 300 m earlier. Some of the other riming reports with V > 300 m may be due to riming occurring between observations with a low ambient visibility, but at the time of the observation the visibility had risen to several hundred metres. Discussions with an experienced observer have revealed that rime deposition will be reported even if the visibility has risen substantially, so long as rime can still be seen.

In order to confirm that the results of the Heathrow analysis are generally applicable and not just a manifestation of reporting practices at Heathrow, the analysis has been repeated for Gatwick and Manchester Airports. The statistics for the two stations are shown in Appendix A, together with a

repeat of the Heathrow statistics. The equivalent tables in Appendix A to Tables 1 and 2 exhibit the same key features i.e. the significance of a visibility threshold around 200 m for rime deposition and the decrease in percentage of rime reports as the temperature approaches zero. The most noticeable difference is that in the analogues of Table 2 the percentage of rime reports decreases more regularly as the temperature approaches zero. Appendix A also contains tables with the aggregated data from all three stations.

3.2 Fog Episodes and Unnecessary De-icing Events

Although the analysis of the number of hourly reports of fog has proved illuminating it is not directly relevant to the estimation of the number of unnecessary de-icings. This requires an estimate of the yearly average number of fog episodes. Since fogs can form in the late evening and persist through midnight, the number of calendar days with fog is not the most useful statistic. To overcome this problem a fog episode has been defined to start when there has been gap of at least 6 hours since the visibility was less than 1000 m. The riming and non-riming SYNOP reports were considered together in defining a fog episode.

A separate count was made of the number of sub-zero fog episodes during which only rime deposition was reported, episodes during which only no rime deposition was reported and episodes during which both were reported. In the latter case it was noticed that often non-riming fog was reported at first as the visibility fell below 1000 m, riming was reported during the middle of the episode and non-riming fog reported as the fog started to dissipate. For the purposes of estimating the potential number of wasted de-icings it is assumed that if rime deposition was reported at any time during a fog episode then de-icing was necessary. Sub-zero episodes with no reports of riming are considered to have led to a wasted de-icing.

Considering first Heathrow, during the 20-year analysis period there were 8 episodes with only reports of rime deposition, 32 episodes with a mixture of reports rime deposition and no deposition and 46 episodes with no reports of fog depositing rime. If the latter are taken as accurate, then there would be around 2 wasted de-icings every years at Heathrow.

The number of sub-zero fog episodes at Gatwick over the same 20-year period was between 2 and 3 times larger. There were 9 episodes with only reports of rime deposition, 71 episodes with a mixture of reports of rime deposition and no rime deposition and 171 episodes with no rime deposition reported at all. The latter statistic implies 8 - 9 wasted de-icings per year. Examination of the individual observations for Gatwick suggested that there were more episodes comprising just one or two observations than at Heathrow. If just one observation of non-riming fog can necessitate de-icing, then the above estimate of wasted de-icings stands. If a longer run of freezing fog observations is required then the estimate will have to be revised.

A possible problem with the method of estimating the number of wasted de-icings is that it assumes the observations of riming are correct. A more conservative estimate has been made allowing for the difficulty in making an observation of riming. The worst case scenario has been assumed in that if riming was reported this is accepted as true. However, if no riming was reported during a fog episode, the visibility and temperature have been examined to see if riming was likely at some time during the episode. For the purposes of the analysis it was assumed that riming occurs if $V < 300$ m and $T \leq -1\,^{\circ}\mathrm{C}$. This reduces the number of non-riming freezing fog episodes at Heathrow from 46 to 24 (around 1 per year) and at Gatwick from 171 to 111 (5 - 6 per year).

4. The Relationship Between Visibility and Liquid Water Content

Given that the analysis of synoptic observations suggests unnecessary de-icings are likely, the next question considered is how well can fog liquid water content be estimated from the visibility data which are routinely available at main airports. A theoretical analysis is performed in this section and the results confirmed by comparison with published observations in Section 5.

The detailed equations relating visibility and LWC are described in Appendix B. The simplest expression is -

$$LWC = (2 r\rho_l)/V \quad \text{----------(1)}$$

where ρ_l is the density of water and r is a drop radius. Equation (1) is fairly exact so long as the drops are all the same size. If there is a range of drops sizes, as would normally be expected, then equation (1) is still fairly exact if r represents the effective radius (r_e). The effective radius can be calculated from the drop size distribution as shown in Appendix B. Equation (1) is less accurate if applied to haze droplets and these will be ignored in the initial calculation. Table 3 shows the LWCs from Eq. (1) for a likely maximum range of r_e. Table 3 shows that for a given visibility fogs comprising large drops have a higher liquid water content. It also indicates the maximum uncertainty in LWC due to variations in r_e, e.g. for V = 200m the LWC can range from 0.05 to 0.17 gm^{-3}.

Table 3 Fog Liquid Water Contents in gm^{-3} for Various Visibilities and Drop Sizes from Eq.(1)

re(μm)	5	7	9	11	13	15	17
Vis (m)							
50	0.20	0.28	0.36	0.44	0.52	0.60	0.68
100	0.10	0.14	0.18	0.22	0.26	0.30	0.34
200	0.050	0.070	0.090	0.11	0.13	0.15	0.17
300	0.033	0.047	0.060	0.073	0.087	0.10	0.113
400	0.025	0.035	0.045	0.055	0.065	0.075	0.085
500	0.020	0.028	0.036	0.044	0.052	0.060	0.068
600	0.017	0.023	0.030	0.037	0.043	0.050	0.057
700	0.014	0.020	0.026	0.031	0.037	0.043	0.049
800	0.013	0.018	0.023	0.028	0.033	0.038	0.043
900	0.011	0.016	0.020	0.024	0.029	0.033	0.038
1000	0.010	0.014	0.018	0.022	0.026	0.030	0.034

The results in Table 3 are plotted in Figure 1a for every other r_e value. This emphasises how the LWC rapidly increases as the visibility falls below 200 m, in accord with the analysis of the synoptic observations.

The theory of the effect of haze droplets on visibility is discussed in detail in Appendix B. Inclusion of their effect lowers the LWC estimate for a given visibility. This is only an extension of the trend apparent in Table 3. The haze droplets having an $r_e < 1$ μm can produce a moderate effect on visibility whilst containing negligible liquid water content. Table 4 shows the results of including a

fairly exact calculation for haze droplets with radius less than 1.5 μm whilst using Eq. (1) for larger drops. The haze droplet size distribution was calculated from CCN concentration measurement in polluted air (Hudson, 1980). Details of the calculation are given in Appendix B. The results in Table 4 are plotted for every other r_e value in Figure 1b. This shows that the largest percentage reduction in LWC values occurs for the higher visibilities and there is only a small reduction in the higher LWC estimates. For example, with r_e = 11 μm, V = 100 m, LWC is reduced by 10% but at 500 m it is reduced by 50%. Another way of looking at this is that for r_e = 11μm an LWC of 0.05 gm^{-3} is now associated with a visibility around 300 m instead of around 450 m.

Table 4 Fog LWC Values in gm^{-3} for Various Visibilities and Drop Sizes Including the Effect of Haze droplets.

r_e (μm)	5	7	9	11	13	15	17
Vis (m)							
50	0.19	0.27	0.34	0.42	0.49	0.57	0.65
100	0.091	0.13	0.16	0.20	0.23	0.27	0.31
200	0.041	0.057	0.072	0.088	0.10	0.12	0.14
300	0.024	0.033	0.042	0.051	0.060	0.069	0.078
400	0.016	0.022	0.027	0.033	0.039	0.044	0.05
500	0.011	0.015	0.018	0.022	0.026	0.029	0.033
600	0.008	0.010	0.012	0.015	0.017	0.019	0.022
700	0.005	0.007	0.008	0.009	0.011	0.012	0.014
800	0.004	0.004	0.005	0.006	0.006	0.007	0.008
900	0.002	0.002	0.002	0.002	0.003	0.003	0.003

Whilst most of the literature surveyed for this report suggested that the haze droplet concentration assumed for Table 4 represented a typical high concentration, a few papers have reported much higher concentrations. The effect is produce a fog with both a very low visibility and liquid water content. For example, Garland et al. (1973) present measurements from one case at Cardington near Bedford, UK which show droplets with $r < 3$ μm contributing up to 50% of the extinction coefficient (the visibility is inversely proportional to the extinction coefficient, see Appendix B), so that an LWC of 0.05 - 0.08 gm^{-3} was associated with a visibility around 60m. (With the CCN concentration used to calculate Table 4, droplets up to 3 μm radius would contribute about 10% of the extinction coefficient with a visibility around 60 m). Zihua et al. (1994) give a similar example from a polluted region of China where the visibility was reduced to 30 - 50 m when the fog LWC was only around 0.03 gm^{-3}. The Clean Air Act should render such cases exceptionally rare now. Also, since for safety purposes we are more interested in maximum LWC values, the ranges given in Tables 3 and 4 seem more appropriate.

5. Comparison with Observations

The calculated values of LWC in Tables 3 and 4 can be compared with the range of observed values obtained from a survey of the literature which is presented in Table 5. Most of the ranges are of are individual measurements. A few values are averages for a case and this is indicated. The methods of measuring LWC and visibility are summarised in Appendix C. Estimates of r_e are also shown in Table 5.

Table 5 Summary of Fog Liquid Water Content Measurements from the Scientific Literature

Source	LWC (gm^{-3})	Visibility (m)	r_e (μm)
Garland et al. (1973)	0.04 - 0.22	230 - 42	-
Low (1975)	0.04 - 0.65	1000 - 84	9.2 - 18.5
Pilie et al. (1975)	0.025 - 0.21	-	Up to 14
Roach et al. (1976)	0.04 - 0.26	-	-
Pinnick et al. (1978)	Up to 0.4 (aloft)	Min vis. 30	-
Brown (1980)	0.15 - 0.48	113 - 38	-
Mack et al. (1980)	0.023 - 0.21 (at 5m) 0.075 - 0.365 (at 44m)	900 - 103 (at 5m) 250 - 75 (at 44m)	7.5 - 15 (at 5m) 5.5 - 12 (at 44m)
Kunkel (1982)	0.047 - 0.24 (case av.) 0.02 - 0.52* (points)	453 - 68 (case av.) 1500 - 36 (points)	5.3 - 12.4 (case av.) 5.0 - 15 (points)
Dollard et al. (1983)	0.057 - 0.23	-	-
Jiusto et al. (1983)	0.03 - 0.50	814 - 75	3.8 - 7.3
Wendisch et al. (1998)	0.092 - 0.31 (case av.)	-	5.8 - 11.0

* Corrected LWC values only go to 0.3 gm^{-3} but uncorrected values are given in Table 5 because only uncorrected visibilities are available.

Table 5 shows an overall LWC range of 0.02 - 0.65 gm^{-3} for a visibility range of 1500 to 38 m. The estimates of r_e vary from 3 to 18.5 μm. However, the largest LWC values only appear in a few references and generally LWC < 0.4 gm^{-3} say, with r_e typically 5 - 15 μm. Thus, the combination of low visibility and large r_e producing large LWC in the top right corners of Tables 3 and 4 seem rare in nature. One likely reason is that such a combination will promote the development of drizzle drops. Rosenfeld and Lensky (1998) have found that for liquid water clouds in general, precipitation-sized drops are generally present once r_e exceeds 14 μm. These would fall out of the fog, capturing fog droplets and reducing the liquid water content. Also, the large fog droplets will have a significant fall speed of their own and this will tend to reduce the fog liquid water content as they settle towards the surface.

Some of the observational references allow extraction of individual LWC, visibility paired values. About 120 pairs have been extracted and these are shown plotted in Figure 2 in the same format as Figure 1. These follow closely the form of the theoretical curves. Below about 175 m visibility the values seem to lie along two lines with a gap between, which presumably would be filled in if many more data points were available. The line of high LWC data points comes from Low (1975) where r_e values up to 18.5 μm were common.

Of particular interest is the LWC associated with higher visibilities, where it may be possible to say ice accretion will be negligible. Eleven values have been extracted with visibility between 500 and 1000 m and these have LWC values in the range 0.02 - 0.07 gm^{-3}. The largest values come from Low (1975) who also observed the largest drop sizes. Otherwise the maximum value is 0.05 gm^{-3}. Heinztenberg et al. (1998) measured much lower LWCs in this visibility range, median value 9.4×10^{-4} gm^{-3}, upper quartile 3×10^{-3} gm^{-3}. There appear two reasons for the much lower LWC values. First, Heinztenberg et al. (1998) made measurements in a polluted region of North Italy. Secondly, their visibility data were obtained from a transmissometer and hence contained the effect of all haze droplets. Their LWC data were obtained from drop-size distributions. Presumably in the polluted atmosphere sampled, nearly all the reduction in visibility was due to droplets beneath the minimum size measured. For the 11 data pairs quoted above with much larger LWC values, both visibility and LWC were derived from the drop-size distribution, so the contribution of small haze droplets to the

visibility was excluded. Thus, the results of Heinztenberg et al. (1998) should be more comparable with Table 4 and Fig. 1b and the rest with Table 3 and Fig 1a. This can be seen to be the case.

The data in Table 5 were obtained at a variety of temperatures and often this was not given in the reference. It was not possible to find a body of LWC data relating specifically to supercooled fog. Presumably, for the wintertime data the temperature should not have been too far above freezing. However, the data presented in Kunkel (1982) were obtained in summer with ambient temperatures up to about 20°C. There is a case for expecting lower liquid water contents in fogs at lower temperatures. This is based on the fact that the amount of condensation in a saturated atmosphere for a given decrease in temperature is less at lower temperatures. Table 6 shows the condensation for a 1°C temperature decrease as a function of temperature, relative to the value at 5°C. It can be seen that the LWC condensed in cooling from -5 to -6°C is half that condensed cooling from 5 to 4°C. However, this is not the only factor controlling fog LWC, so it is not clear how much temperature will affect actual fog LWC values. For example, part of the cooling generating condensation in fog is offset by the latent heat released by condensation. The offsetting will be less at lower temperatures because of the reduced condensation rate. Therefore, the fog may cool more at lower temperatures producing more condensation.

Table 6 Condensation per Degree Cooling, Relative to the Value at 5 - 4°C

Temperature (°C)	21 - 20	15 - 14	11 - 10	5 - 4	0 - -1	-5 - -6
Relative Condensation	2.52	1.77	1.43	1.0	0.78	0.52

6. Illustrative Examples of Ice Deposition Rates

Various scenarios are assumed in this section in order to convert the LWC values in Table 3 into plausible accretion rates, which should be more meaningful to the aviation community. The results are stratified by visibility and drop size to help the reader judge whether there is a visibility threshold beyond which deposition rate may be insignificant for any drop size. It should noted that because the author is not an expert on the theory of deposition on aerofoils, the results should be considered as illustrative only. The FAA Aircraft Icing Handbook (1991) has been used for these calculations and details are given in Appendix D.

Fog droplets may impact on a surface in two ways. The simplest is by falling onto the surface under the action of gravity. Only a basic calculation is required to show that this produces very low accretion rates. The droplet fall speed varies as r^2 for fog droplets and ranges from 0.3 cm s^{-1} for a 5 μm radius droplet to 2.7 cms^{-1} for a 15 μm radius droplet. Assuming a droplet fall speed of 2.5 cms^{-1} and an LWC of 0.6 g m^{-3} (i.e. r_e around 15 μm and visibility around 50 m) the deposition rate of water is 54 g m^{-2} per hour. Assuming the density of ice is 0.8 g cm^{-3}, this translates into a deposition rate of 0.068 mm h^{-1}. The settling of fog droplets under gravity acts to reduce fog liquid content, Brown and Roach (1976), so a fog depositing water at this rate would be unlikely to maintain such a high LWC and hence high deposition rate for very many hours.

The other method of deposition occurs when the fog droplets being carried along at the ambient wind speed impact on a surface, or equivalently are captured by an aircraft in motion. Only a fraction of the droplets upstream of an object impact upon it in general. As the streamlines of airflow diverge around an object, the smallest droplets may follow the airflow and miss the object. The larger droplets have higher inertia i.e. a greater tendency to keep moving in a straight line. They depart from the streamlines of the flow and may impact on the object. The collection efficiency (E) of an object is the fraction of liquid water directly upstream of the object which is captured. The collection efficiency increases as the object size decreases, the drop size increases and the air speed increases.

The LWC values in Table 3 have been used for sample calculations of the deposition rate in fog assuming a surface wind speed of 2 ms^{-1}, a reasonably large value for radiation fog. The calculations have been performed for a 1 cm diameter cylinder and a NACA aerofoil with a chord length of 3.1 ft, the typical dimensions of a stabiliser according to the FAA Aircraft Icing Handbook. Details of the calculation are given in Appendix D. The results are shown in Table 7 together with deposition rates for unit collection efficiency. The zeroes for the cylinder indicate deposition rates less than hundredth of a mm per hour whilst the dashes for the aerofoil indicate zero deposition. For reasons explained in Appendix D, the values for the cylinder are average deposition rates i.e. assuming a uniform thickness, whilst for the aerofoil they are the maximum deposition rate. The results in Table 7 for E = 1 and for the cylinder are plotted in Figure 3.

Table 7 Ice Deposition Rates in mmh^{-1} for a 2 ms^{-1} Wind Speed and Ice Density 0.8 gcm^{-3}

Radius	5 μm			10 μm			15 μm		
Vis. (m)	E=1	Cylinder D = 1cm	Aerofoil c = 3.1ft	E=1	Cylinder D = 1cm	Aerofoil c = 3.1ft	E = 1	Cylinder D = 1cm	Aerofoil c = 3.1ft
50	1.8	0.01	-	3.6	0.82	-	5.4	1.9	0.65
100	0.90	0.01	-	1.8	0.41	-	2.7	0.94	0.32
200	0.45	0.00	-	0.90	0.21	-	1.35	0.47	0.16
300	0.30	0.00	-	0.60	0.14	-	0.90	0.31	0.11
400	0.23	0.00	-	0.45	0.10	-	0.68	0.24	0.08
500	0.18	0.00	-	0.36	0.08	-	0.54	0.19	0.06
600	0.15	0.00	-	0.30	0.07	-	0.45	0.16	0.05
700	0.13	0.00	-	0.26	0.06	-	0.39	0.13	0.05
800	0.11	0.00	-	0.23	0.05	-	0.34	0.12	0.04
900	0.10	0.00	-	0.20	0.05	-	0.30	0.10	0.04
1000	0.09	0.00	-	0.18	0.04	-	0.27	0.09	0.03

The key result apparent in Table 7 and Figure 3 is the dependence on drop size and object size. The variation with drop size for E = 1 merely reflects the variation of LWC with radius for a given visibility. A much larger variation occurs for the cylinder and aerofoil because of the variation of E with drop size. With r = 5 μm there is negligible deposition on a 1 cm diameter cylinder and none on the aerofoil. For r = 10 μm the deposition rate on the cylinder is about a quarter of that for E = 1 but still equals zero for the aerofoil. At r = 15 μm there is some deposition on the aerofoil. These calculations will tend to overestimate the effect of drop size because drops of one size are assumed. If the radii were considered to be a mean value, then larger drops would be present, with higher collection efficiencies. In view of the uncertainties in the calculation, it was not considered worthwhile to introduce the complexity of using a drop-size distribution at this time. However, Table 7 does show that deposition would only occur on the 3.1 ft chord aerofoil in fogs containing larger droplets, according to the theory in the FAA Handbook. The latter caveat is added, not as a criticism of the treatment, but because it applies to the aircraft in flight. The airflow in flight will be towards the leading edge of the aerofoil. In a fog the wind may make any angle with the aerofoil.

An estimate of the possible accretion during taxiing and take off has also been made. In this case we are not interested in hourly deposition rates but in the accretion as the aircraft traverses a finite distance. The calculation was split into a taxiing and take off stage. It was assumed that the aircraft taxied for 2 km at 10 ms^{-1}, then took off over a distance of 2 km at a mean speed of 100 ms^{-1}. The accretion rates during taxiing are shown in Table 8 and during take off in Table 9. They are shown as a function of visibility, for three drop sizes, using LWC values from Table 3.

Table 8 Deposition in mm on a NACA 0012 Aerofoil of 3.1 ft Chord During Taxiing

Radius (μm)	5	10	15
Visibility (m)			
50	0.00	0.28	0.68
100	0.00	0.14	0.34
200	0.00	0.07	0.17
300	0.00	0.05	0.11
400	0.00	0.04	0.08
500	0.00	0.03	0.07
600	0.00	0.02	0.06
700	0.00	0.02	0.05
800	0.00	0.02	0.04
900	0.00	0.02	0.04
1000	0.00	0.01	0.03

Table 9 Deposition in mm on a NACA 0012 Aerofoil of 3.1 ft Chord During Take Off

Radius (μm)	5	10	15
Visibility (m)			
50	0.20	0.64	1.13
100	0.10	0.32	0.56
200	0.05	0.16	0.28
300	0.03	0.11	0.19
400	0.02	0.08	0.14
500	0.02	0.06	0.11
600	0.02	0.05	0.09
700	0.01	0.05	0.08
800	0.01	0.04	0.07
900	0.01	0.04	0.06
1000	0.01	0.03	0.06

The higher velocities, especially during take off, produce much higher capture efficiencies than when the aircraft is stationary, so there is some deposition for every drop size shown during take off. However, there is still a strong dependence on drop size. The accretion during take off is about twice that during taxiing for the 10 and 15 μm radius drops and it is the entire contribution for 5 μm radius drops. For r = 15 μm, taxiing plus take off contributes a similar deposition to the effect of a 2 ms^{-1} wind speed acting over three hours. For the lower two drop sizes it is the entire contribution.

7. Instrumentation to Measure Liquid Water Content and Drop Size

With synoptic observations suffering from the inherent difficulty of judging whether riming is occurring and the uncertainty in LWC values derived from visibility, this section considers the possibility of automated measurements. There are three types of measurement which can be considered. Rosemount manufacture an instrument which measures the rate of accretion of ice on a small probe. This would appear to be an obvious choice but according to Laforte et al. (1995) the

basic probe has several problems. The alternative is to make direct measurements of LWC or drop size. However, such measurements are difficult to make accurately and as far as the author is aware are not made routinely at the surface. The instrumentation is generally designed for air-borne use in cloud physics research and is also now used by aircraft manufacturers during certification flights. This means that many of the instruments are designed to work at airspeeds in excess of 80 mph. Regular calibration and servicing is generally required to maintain accuracy.

A brief review of the most common instruments is now given. More details may be found in the FAA Aircraft Icing Handbook (1991) and the references in sections 7.1 - 7.3.

7.1 The Rosemount Icing Probe

The Rosemount Icing Probe is manufactured as a variety of models. Basically, it consists of a probe about 6 mm in diameter and 25 mm long which is vibrated longitudinally at a nominal 40,000 Hz. When ice accretes upon it the vibrational frequency decreases, approximately linearly with mass of ice accreted. When the frequency decrease reaches a predetermined amount, around 350 Hz, a heater is switched on to melt the ice and a warning can be triggered. After heating for typically 90 s, the probe cools and the cycle starts over again. The rate of ice accretion, averaged over a time period, is determined from the number of heating cycles, with allowance being made for the dead time during heating and cooling down again. It also appears to be possible to obtain a more instantaneous estimate of accretion rate from the rate of change of frequency with time but it is not clear whether the standard instrument can do this.

The Rosemount probe is basically made as a warning device, which may be all that is required for the freezing fog scenario. Claffey et al. (1995) have successfully obtained LWC from the probe in wind tunnel tests. However, this needs a knowledge of drop size and wind speed to calculate the capture efficiency and does not seem a sensible way to proceed.

As an off-the-shelf system it is tempting to look no further. However, Laforte et al. (1995) describe several problems with the basic system. The reference frequency can drift in time triggering false alarms. This appears to be because the difference from the nominal baseline frequency is measured rather than from the actual baseline frequency. Water from the melted ice can remain on the probe and refreeze, triggering another alarm too soon. Laforte et al. (1995) describe an instrument they have developed based on a Rosemount Probe for monitoring rime deposition on power lines. They measure the actual baseline frequency and determine the drift from this. They have also introduced an electro-mechanical system for shaking water off the probe after heating. They say that the modified system is used at a network of stations in Quebec, Canada. Unfortunately, they only describe wind tunnel tests, not operational experience. Neither do they state whether the modified probe is available commercially.

A key question is how well does the probe operate at low windspeeds. Laforte et a. (1995) tested it down to 5 ms^{-1}. There appears nothing in the principle of operation of the probe to stop it functioning at any windspeed. The main question mark is over sensitivity. At very low wind speeds both the flux of water impinging on the probe and the capture efficiency will be reduced. The wind tunnel tests of Claffey et al. (1995) and Laforte et al. (1995) on several models give 45 - 65 mg of ice accreted to trigger the heater.

7.2 LWC Instruments

The two instruments most commonly used to make continuous LWC measurements are the Johnson-Williams Probe and the CSIRO Probe (the latter is also known as the King Probe). Both instruments work by measuring the effect of evaporative cooling as the droplets impinge upon a heated wire. The J-W probe measures the change in resistance of the wire whilst the CSIRO probe measures the current required to maintain the wire at a constant temperature. Both instruments have to allow for heat lost from the wire by convection to the air. The CSIRO probe uses a theoretical correction whilst the J-W Probe has a second heated wire placed parallel to the flow so that no droplets impinge upon it. Both instruments have a range up to 3 gm^{-3}. The J-W Probe works over the airspeed range 80 - 200 MPH and the CSIRO Probe 140 - 230 MPH. Strapp and Schemenauer (1982) found that about 75% of J-W Probes tested in a wind tunnel were accurate to 20%. However, they required careful calibration before use to achieve this. A key problem with J-W probes is that they suffer from baseline drift (i.e. give finite liquid water contents in clear air) and require frequent adjustment to avoid this. The accuracy of the CSIRO Probe is around 5% at 1 gm^{-3} according to King et al. (1985) and it has less of a problem with baseline drift.

Jiusto and Lala (1983) report a promising remote sensing technique using an infrared laser working at 10.6 μm. It is essentially a transmissometer as used to measure visibility, but measures the extinction coefficient at 10.6 μm instead of at visible wavelengths. The technique is based upon the theoretical study of Chylek (1978). This showed that at infrared wavelengths around 8 - 13 μm, the extinction coefficient is proportional LWC, independent of the drop-size distribution. This is in marked contrast to visible wavelengths where there is a strong dependence as shown by Table 3. A simple explanation of this behaviour is given in Appendix B. Jiusto and Lala (1983) used $\beta_{10.6} = 145LWC$ where $\beta_{10.6}$ is the measured extinction coefficient at 10.6 μm in Km^{-1} and LWC is in gm^{-3}. They report good agreement with direct weighing measurements of LWC in fogs with LWC up to 0.4 gm^{-3}. The main limitation of this technique is that the linear relationship becomes less accurate as the proportion of drops larger than 14 μm increases. Also, the author is not aware of it having been exploited to produce a commercial instrument.

Gerber Scientific Inc. manufacture a laser diffraction instrument one version of which measures LWC directly (PVM - 100), Gerber (1991). This has been field tested on a mountain site for 3 weeks during which there were 50 Kt winds, rain, graupel, snow and the temperature fell to -10°C. Despite the challenging conditions, the baseline drift was negligible according to Gerber (1991). The LWC from the PVM agreed with that from an FSSP droplet spectrometer (described in Section 7.3) to within 10%. Unfortunately less good performance was reported by Wendisch et al. (1998). They compared 5 PVM instruments and found differences of up to 40% in the LWC values from each instrument. However, since the differences were constant in time they could be corrected by calibration. A more serious problem was revealed by comparing PVM LWC with LWC derived from an FSSP droplet spectrometer. The comparison showed a systematic underestimate by the PVM as the effective radius of the drop-size distribution exceeded 8 μm. The underestimate increased with increasing r_e up to a factor of 6 to 8. Wendisch et al. (1998) suggested that a possible cause is that the PVM is less sensitive to larger drops. This would be particularly unfortunate for monitoring riming.

7.3 Drop-Size Measurements

The standard device for measuring drop size and concentrations used by the cloud physics community is the Forward Scattering Spectrometer Probe (FSSP), manufactured by Particle Measuring Systems Inc. , Boulder. This measures drop sizes and concentrations in 15 size classes up to 23.5 μm radius. The LWC can also obtained by integrating over the drop-size distribution (see Appendix B, Eq. (10)). It has the key advantage over the hot wire LWC probes of working down to

airspeeds of a few metres per second and has been used at the surface in many fog studies. It works by measuring the light scattered from individual drops as they pass through a laser beam. The sample volume of the beam is small enough to minimise the possibility of there being more than one drop at a time in the beam. At concentrations above 500 cm^{-3} it is necessary to correct for drop coincidences within the beam. Drop size accuracy is no better than 10% and LWC accuracy is around 35%. Although this is less accurate than the best performance of the hot-wire LWC probes, the accuracy of the FSSP may hold up better during prolonged unattended use. The main problem in prolonged use is dirt gathering on the optics. It is also critical that the laser remain optically aligned. The cloud physics community generally perform routine calibration using glass beads or water drops of a known size generated by an ultrasonic droplet generator.

7.4 Conclusions on the Choice of Instrumentation

The most promising instrument appears to be the modified Rosemount Probe developed by Hydro Quebec as reported by Laforte et al. (1995). However, the author has no personal experience of this and it is not clear if it available commercially.

The second choice is between an FSSP to measure the drop-size distribution and a PVM to measure LWC directly. They both have the advantage of being available commercially and of working on the ground. Besides the basic FSSP, it would be necessary to purchase a data acquisition system to process the FSSP data. One can integrate the drop-size distribution to obtain the LWC. Combining the effective radius from the FSSP with the output from the transmissometer used to measure visibility would produce another estimate of LWC and would exploit the much larger sample volume of the transmissometer. It may also improve the accuracy of the LWC estimate since it would only require effective radius from the FSSP, accuracy around 10%, whilst the FSSP LWC is only accurate to around 35%. The disadvantage is that significant development may be required to automatically combine the information from the two instruments. The PVM has the advantage of giving LWC directly without further processing. Since it is a newer instrument than the FSSP, there is less information on its performance available. Before being selected it is recommended that more information is obtained on its performance when the LWC is contained in large drops.

The infrared transmissometer technique would be an elegant solution but would have to be designed and manufactured, presumably at far greater cost than a commercially available instrument. The first step in taking this technique further would be to estimate the accuracy of the underlying theory for fogs containing large drops.

In order to use the hot wire LWC probes they would have to installed in small wind tunnels where the air was accelerated to their operating speed. This seems the least viable option.

8. Conclusions

The scope of the unnecessary de-icing problem has been examined by an analysis of hourly observations from Heathrow, Gatwick and Manchester airports. Comparison of the weather type in the SYNOP report (i.e. fog depositing rime or fog not depositing rime) with the reported visibility and temperature shows -

(i) The proportion of fogs with riming increases as the visibility falls to 200 m or less and the temperature falls farther below 0°C . If the visibility is 200 m or less, from 0 to -1°C around 40% of fogs have rime deposition reported and this rises to 84% if the temperature is below -3°C.

(ii) A minority of the observations are inconsistent with the estimated range of likely fog liquid water contents and ice deposition rates. The uncertainty in the observations reflects the

difficulty of making a visual observation of rime deposition. For greater certainty it would be necessary to make an instrumental measurement of rime deposition or liquid water content.

To estimate the potential number of wasted de-icings, the hourly observations have been combined into episodes of supercooled fog by insisting on a gap of at least 6 hours without a supercooled fog report between episodes. Assuming that a de-icing would take place after just one report of freezing fog according to the METAR code (i.e. $T < 0^{o}C$ and $V < 1000$ m), there would be between 1 and 2 wasted de-icings a year at Heathrow and between 4 and 9 at Gatwick. The range in the estimate arises from the uncertainty in the reported observations of riming and could probably only be refined by acquiring instrumented records over many years.

Theory and observations are in accord that one can only infer fog liquid water content from the visibility to within a factor of 2 - 3. The reason is that for a given liquid water content the visibility depends on the size of the fog droplets. For greater precision, the LWC or riming rate would have to be measured directly.

Estimates of deposition rates of rime on a 1 cm diameter cylinder and 3.1 ft chord aerofoil as examples show -

(i) Deposition due to direct settling of the fog droplets under gravity appears insignificant (< 0.07 mmh^{-1}).

(ii) At typical windspeed in radiation fog, riming due to droplets moving with the wind is only significant for smaller objects and according to the basic theory does not occur at all on the aerofoil unless larger fog drops are present.

(iii) The rate of ice accretion is sensitive to drop size and increases with increasing drop size.

(iv) The elementary calculations for the aerofoil suggest that for fogs without larger droplets, nearly all the deposition occurs during taxiing and take off. For large droplet fogs, riming whilst parked for several hours can make an equal contribution.

From a review of instrumentation which can make measurements of either riming, LWC or drop size it is concluded that the most promising instrument is the modified Rosemount Icing Probe developed by Hydro Quebec. Since it is not known if this is commercially available, also worth further investigation are the Forward Scattering Spectrometer Probe which measures drop size and LWC and the PVM device which measures LWC. Both are available commercially. Only the cost of the FSSP is known at present and this is around £35K.

It should be noted that several uncertainties remain, which could not be addressed within the budget of the study. First, fog LWC can increase with height, especially over the first 50 m above the surface e.g. Pinnick et al. (1978), Mack et al. (1980). In the latter reference, the maximum reported LWC was 0.21 g m^{-3} at 5 m height but 0.365 gm^{-3} at 44 m. Some allowance for this ought to be made in estimating overall fog LWC from surface measurements. Secondly, drizzle will form in thick fogs, especially if r_e is large. This will enhance the ice deposition rate due to direct settling of the drops onto the aircraft. It may also produce a rougher ice surface. The final uncertainty is that prior to fog formation, conditions will be conducive to dew deposition on the aircraft. If the temperature falls below $0^{o}C$, this may freeze to form ice, even though the visibility remains too high for significant ice deposition from fog drops.

Despite the uncertainties, the overall conclusion is that wasted de-icings must occur. In order to take this further, the key issues appear to be -

(i) Is there a visibility threshold (< 1000 m) above which deposition is negligible, even for fogs comprising large drops.

(ii) If there is a range of visibilities such that deposition is negligible for small-drop fogs but significant for large-drop fogs, is it cost effective to introduce instrumentation to measure riming rate, LWC or drop size operationally.

9. Acknowledgement

I wish acknowledge the assistance given by Keith Grant (C Division) who provided the basic fog statistics for the three stations and with whom I had useful discussions on their interpretation.

10. References

Brown, R., 1980: A numerical model of radiation fog with an explicit formulation of the microphysics. Quart. J. R. Meteor. Soc., **106**, 781 - 802.

Brown, R. and W. T. Roach, 1976: The physics of radiation fog: II - a numerical study. Quart. J. R. Meteor. Soc., **102**, 335 - 354.

Chylek, P., 1978: Extinction and liquid water content of fogs and clouds. J. Atmos. Sci., **35**, 296 - 300.

Claffey, K. J., K. F. Jones and C. C. Ryerson, 1995: Use and calibration of Rosemount ice detectors for meteorological research. Atmospheric Res., **36**, 277 - 286.

Dollard, G. J. and M. H. Unsworth, 1983: Field measurements of turbulent fluxes of wind-driven fogs to a grass surface. Atmospheric. Environment, **17**, 775 - 780.

Eldridge, R. G., 1971: The relationship between visibility and liquid water content in fog. J. Atmos. Sci., **28**, 1183 - 1186.

FAA, 1991: Aircraft Icing Handbook. DOT/FAA/CT-88/8-1

Garland, J. A., 1969: Condensation on ammonium sulphate particles and its effect on condensation. Atmospheric Environment. **3**, 347 - 354.

Garland, J. A., J. R. Branson and L. C. Cox, 1973: A study of the contribution of pollution to visibility in a radiation fog. Atmospheric Environment, **7**, 1079 - 1092.

Gerber, H., 1991: Direct measurements of suspended particulate concentration and far-infrared extinction with a laser-diffraction instrument. Applied Optics, **30**, 4824 - 4831.

Heintzenberg J., M Wendisch, B. Yuskiewicz, D. Orsini, A. Wiedensohler, F. Stratmann, G. Frank, B. G. Martinsson, D. Schell, S. Fuzzi and G. Orsi, 1998: Characteristics of haze and fog. Contr. Atmos. Phys., **71**, 21 - 31.

Howell, D. B., 1969: Angular scattering functions for spherical water droplets. Naval Res. Lab., Washington, D. C., NRL Report 6955.

Hudson, J. G., 1980: Microphysics of coastal fogs and stratus. Proc. 8th Int. Conf. on the Physics of Clouds, Clermond-Ferrand, **1**, 205 - 208

Jiusto, J. E. and G. G. Lala, 1983: Radiation fog field programs - Recent studies. Atmospheric Sciences Research Center, State University of New York, Albany, Pub. No. 869.

King, W. D., J. E. Dye, J. W. Strapp, D. Baumgardner and D. Huffman, 1985: Icing wind tunnel tests on the CSIRO liquid water probe. J. Atmos. Oceanic Technology, **2**, 340 - 352.

Kunkel, B. A., 1982: Microphysical properties of fog at Otis AFB. Air Force Geophysics Lab., Hanscom AFB, Report No. AFGL-TR-82-0026.

Laforte, J. L., M. A. Allaire and J. Laflamme, 1995: Wind tunnel evaluation of a rime metering device using a magnetorestrictive sensor. Atmospheric Res., **36**, 287 - 301

Liu, Y. and J. Hallett, 1997: The '1/3' power law between effective radius and liquid-water content. Quart. J. R. Meteor. Soc., **123**, 1789 - 1795.

Low, R. D. H., 1975: Microphysical evolution of fog. J. Rech. Atmos., **12**, 23 - 32.

Mack, E. J., B. J. Wattle, C. W. Rogers and R. J. Pilie, 1980: Fog characteristics at Otis AFB, MA. Air Force Geophysics Lab., Hanscom AFB, Report No. AFGL-TR-80-0340.

Mason, B. J., 1971: The Physics of Clouds. Clarendon Press, Oxford.

Middleton, W. E. K., 1952: Vision Through the Atmosphere. University of Toronto Press, Toronto.

Pilie, R. J., E. J. Mack, W. C. Kocmond, W. J. Eadie and C. W. Rogers, 1975: The life cycle of valley fog. Part II: Fog microphysics. J. Appl. Meteor., **14**, 364 - 374.

Pinnick, R. G., D. L. Hoihjelle, G Fernandez, E. B. Stenmark, J. D. Lindberg and G. B. Hoidale, 1978: Vertical structure of atmospheric fog and haze and its effects on visible and infrared extinction. J. Atmos. Sci., **35**, 2020 - 2032.

Roach, W. T., R. Brown, S. J. Caughey, J. A. Garland and C. J. Readings, 1976: The physics of radiation fog: I - a field study. Quart. J. R. Meteor. Soc., **102**, 313 - 333.

Rosenfeld, D. and I. M. Lensky, 1998: Satellite-based insights into precipitation formation processes in continental and maritime convective clouds. Bull. Amer. Meteor. Soc., **79**, 2457 - 2476.

Starr, J. R., 1967: Inertial impaction of particulates upon bodies of simple geometry. Ann. Occup. Hyg., **10**, 349 - 361.

Strapp, J. W. and R. S. Schemenauer, 1982: Calibrations of Johnson-Williams liquid water content meters in a high-speed icing tunnel. J. Appl. Meteor., **21**, 98 - 108.

Walton and Wallock, 1960: The suppression of airborne dust by water spray. J. Air Pollution, **3**, 129 - 153.

Wendisch, M., S. Mertes, J. Heintzenberg, A. Wiedensohler, D. Schell, W. Wobrock, G. Frank, B. G. Martinsson, S. Fuzzi, G. Orsi, G. Kos, and A. Berner, 1998: Drop size distribution and LWC in Po Valley fog. Contr. Atmos. Phys., **71**, 87 - 100.

Zihua, L., Z. Limin and Z. Qinghong, 1994, The physical structure of the winter fog in Chongqing metropolitan area and its formation process. Acta Meteorologica Sinica, **8**, 316 - 328.

Appendix A Fog Statistics at Heathrow, Gatwick and Manchester Airports Jan. 1977 - Dec. 1996

Gatwick Airport

Total number of observations - **175283**

Total number of observations with T < 0°C - **9026** (5.2%)

Total number of observations with T < 0°C and V < 1000 m - **1235** (13.7% of occasions with T < 0°C)

Total number of observations with T < 0°C and V < 1000 m and rime deposited - **375**

Total number of observations with T < 0°C and V < 1000 m and rime not deposited - **860**

	V < 100 m			V < 200 m		
T (°C)	Rime	No Rime	% Rime	Rime	No Rime	% Rime
< -3.	**48**	**1**	**98**	**99**	**19**	**84**
-3 to -2.1	**27**	**6**	**82**	**54**	**35**	**61**
-2 to -1.1	**25**	**24**	**51**	**64**	**59**	**52**
-1 to -0.1	**9**	**46**	**16**	**22**	**141**	**13**
Total	**109**	**77**	**59**	**239**	**254**	**48**

	200 < V < 1000 m			300 < V < 1000 m		
T (°C)	Rime	No Rime	% Rime	Rime	No Rime	% Rime
< -3	**63**	**116**	**35**	**36**	**85**	**30**
-3 to -2.1	**36**	**108**	**25**	**17**	**80**	**18**
-2 to -1.1	**40**	**164**	**20**	**22**	**125**	**15**
-1 to -0.1	**7**	**218**	**3**	**5**	**144**	**3**
Total	**146**	**606**	**19**	**80**	**434**	**16**

Manchester Airport

Total number of observations - **175139**

Total number of observations with T < 0°C - **6895** (3.9%)

Total number of observations with T < 0°C and V < 1000 m - **690** (10% of occasions with T < 0°C)

Total number of observations with T < 0°C and V < 1000 m and rime deposited - **289**

Total number of observations with T < 0°C and V < 1000 m and rime not deposited - **401**

	V < 100 m			V < 200 m		
T (^{0}C)	Rime	No Rime	% Rime	Rime	No Rime	% Rime
< -3.	**31**	**7**	**82**	**72**	**13**	**85**
-3 to -2.1	**18**	**8**	**69**	**44**	**19**	**70**
-2 to -1.1	**6**	**9**	**40**	**35**	**24**	**59**
-1 to -0.1	**2**	**8**	**20**	**21**	**58**	**27**
Total	**57**	**32**	**64**	**172**	**114**	**60**

	200 < V < 1000 m			300 < V < 1000 m		
T (^{o}C)	Rime	No Rime	% Rime	Rime	No Rime	% Rime
< -3	**57**	**68**	**46**	**33**	**58**	**36**
-3 to -2.1	**20**	**41**	**33**	**12**	**37**	**24**
-2 to -1.1	**28**	**79**	**26**	**17**	**67**	**20**
-1 to -0.1	**12**	**100**	**11**	**8**	**86**	**9**
Total	**117**	**288**	**29**	**70**	**248**	**22**

Heathrow

Total number of observations - **175320**

Total number of observations with T < 0^{o}C - **5491** (3.1%)

Total number of observations with T < 0^{o}C and V < 1000 m **- 539** (9.8% of occasions with T < 0^{o}C)

Total number of observations with T < 0^{o}C and V < 1000 m and rime deposited - **234**

Total number of observations with T < 0^{o}C and V < 1000 m and rime not deposited - **305**

	V < 100 m			V < 200 m		
T (^{0}C)	Rime	No Rime	% Rime	Rime	No Rime	% Rime
< -3.	**36**	**7**	**84**	**48**	**9**	**84**
-3 to -2.1	**18**	**8**	**69**	**55**	**13**	**81**
-2 to -1.1	**23**	**12**	**66**	**65**	**27**	**71**
-1 to -0.1	**15**	**29**	**34**	**38**	**61**	**38**
Total	**92**	**56**	**62**	**206**	**110**	**65**

	200 < V < 1000 m			300 < V < 1000 m		
T (^{o}C)	Rime	No Rime	% Rime	Rime	No Rime	% Rime
< -3	**10**	**30**	**25**	**9**	**27**	**25**
-3 to -2.1	**6**	**46**	**12**	**4**	**37**	**11**
-2 to -1.1	**26**	**43**	**38**	**21**	**37**	**36**
-1 to -0.1	**18**	**74**	**20**	**14**	**55**	**20**
Total	**60**	**193**	**23**	**48**	**156**	**24**

Combined Gatwick, Heathrow and Manchester Airport Tables

	V < 100 m			V < 200 m		
T (^{0}C)	Rime	No Rime	% Rime	Rime	No Rime	% Rime
< -3.	**115**	**15**	**88**	**219**	**41**	**84**
-3 to -2.1	**63**	**22**	**74**	**153**	**67**	**70**
-2 to -1.1	**54**	**45**	**55**	**164**	**110**	**60**
-1 to -0.1	**26**	**83**	**24**	**81**	**260**	**24**
Total	**258**	**165**	**61**	**617**	**478**	**56**

	200 < V < 1000 m			300 < V < 1000 m		
T (^{0}C)	Rime	No Rime	% Rime	Rime	No Rime	% Rime
< -3	**130**	**214**	**38**	**78**	**170**	**32**
-3 to -2.1	**62**	**195**	**24**	**33**	**154**	**18**
-2 to -1.1	**94**	**286**	**25**	**60**	**229**	**21**
-1 to -0.1	**37**	**392**	**9**	**27**	**285**	**9**
Total	**323**	**1087**	**23**	**198**	**838**	**19**

Appendix B Theory of Visibility

1. Koschmeider Theory

The theory of visual range was developed by Koschmeider (1924) and is discussed in detail in Middelton (1952). Koschmeider's theory considers a black object viewed against the sky as a background. The black object has a zero intrinsic luminance by definition but viewed from a range R has finite luminance B_b due to light scattered towards the observer by the intervening atmosphere. If the sky has luminance B_s Koschmeider derived the following relationship -

$$B_b = B_s (1 - e^{-\beta R}) \quad \text{----------} \quad (1)$$

where β is the extinction coefficient which depends on the concentration and sizes of the particles/drops within the atmosphere. As β and R increase the black body appears brighter as more light is scattered towards the observer. The contrast (C) between the black object and the sky may be defined as -

$$C = (B_b - B_s)/B_s \quad \text{----------} \quad (2)$$

As β and/or R increase C decreases as B_b approaches B_s. The visual range (or more colloquially 'visibility') is the range where the contrast is reduced to a limiting value ε at which the eye can no longer distinguish the black body. At this range R = V by definition and -

$$V = \frac{\ln \varepsilon}{\beta} \quad \text{----------} \quad (3)$$

Koschmeider used ε = 0.02 giving $V = 3.9/\beta$ but it is recommended to use ε = 0.05 by WMO giving -

$$V = 3.0/\beta \quad \text{----------} \quad (4)$$

Equation (4) is used in this report, one reason being that it is used in the calibration of Met. Office transmissometers. However, it should be noted that many scientific papers continue to use 3.9 as the numerator.

The exact expression for the extinction coefficient due to drops is -

$$\beta = \pi \int_0^\infty Q(r) n(r) r^2 dr \quad \text{----------} \quad (5)$$

where n(r) is the concentration and Q(r) the scattering efficiency factor for drops of radius r. For droplets with r > 2μm, $Q(r) \approx 2$ so Eq. (5) becomes -

$$\beta = 2\pi \int_0^\infty n(r) r^2 dr \quad \text{----------} \quad (6)$$

Equation (1) of the main text can easily be derived if all the drops are the same size, so that -

$$\beta = 2\pi nr^2 \quad \text{----------(7)}$$

For drops of one size the liquid water content W is given by -

$$W = \tfrac{4}{3}\pi\rho_l nr^3 \quad \text{----------(8)}$$

where ρ_l is the density of water. From Eqs. (4) (7) and (8) -

$$V = \frac{3.0}{2\pi nr^2} = \frac{2r\rho_l}{W} \quad \text{----------(9)}$$

For a size distribution of drops,

$$W = \tfrac{4}{3}\pi\rho_l \int_0^\infty n(r)r^3 dr \quad \text{----------(10)}$$

and using equation (6) one can write -

$$V = \frac{2r_e\rho_l}{W} \quad \text{----------(11)}$$

where $r_e = \dfrac{\int_0^\infty n(r)r^3 dr}{\int_0^\infty n(r)r^2 dr}$

r_e is known as the effective radius and is used widely in the theory of the transfer of solar radiation through the atmosphere. Unfortunately, in the literature on fog the arithmetic mean radius (r_a) is normally used, which is smaller.

2. Allowance for Submicron Droplets

If a fog only contained drops with r > 1 - 2 μm we could safely use Eq. (11) to estimate LWC given V. However, fogs generally contain a significant concentration of unactivated CCN with R < 1 μm. Because $\beta \propto r^2$ and $W \propto r^3$, the drops with r < 2μm make a much more significant contribution to β than to LWC. This is exacerbated by the fact that Q(r) peaks at around 4 when r is around 0.5 μm. Eldridge(1971) gives an example of a drop-size distribution where neglect of droplets with r < 3 μm produces an underestimate of 42% in visibility but only 12% in LWC. For an exact calculation of the visibility one needs to consider the variation of Q(r) with r for r < 2 μm say and not just use a constant value of 2. This has been considered in detail because we wish to see if there is negligible LWC associated with higher visibilities below 1000 m where de-icing may not be necessary. It is for the higher visibilities that the haze droplets will make the most significant contribution relative to the larger drops.

In relating LWC and visibility it is necessary to consider how they were measured. The two most common ways are either that both are obtained from a drop-size distribution or the LWC is obtained

from a drop-size distribution and the visibility is measured directly e.g. with a transmissometer. Occasionally LWC is measured by drawing the droplet laden air into a specially designed jar (an impinger) which is weighed before and afterwards. This will sample all droplet sizes.

Initially, the author thought the effect of haze droplets would be more important than now appears to be the case. This was particularly due to the much quoted paper of Garland et al. (1973) where in a dense fog at Cardington, Bedford, up to half the extinction coefficient was produced by droplets with $r < 3\mu m$. Typically, around 3000 cm^{-3} of droplets were found between 0.6 and 1.2 μm radius, with 6000 cm^{-3} below 0.6 μm radius. The size distributions were measured with oil coated slides using an advanced microscopic technique. More recent references are based on the use of optical particle spectrometers and these report a much lower concentration of haze droplets. The one exception is Zihua et al. (1994) who found that in a polluted city centre in China a visibility of 30 - 50 m was associated with an LWC around 0.03 g m^{-3}. Garland's paper is also internally inconsistent in that the measured CCN concentrations were only 20 - 118 cm^{-3}. Theoretically, they should have been comparable with the haze droplet concentration. In performing calculations to estimate the effect of haze droplets guidance has been obtained from more recent papers.

Kunkel (1982) made measurements using an FSSP droplet spectrometer. Concentrations in the radius range 0.25 - 1.25 μm varied from 100 - 600 cm^{-3}. The concentration of droplets with $r > 1.25\mu m$ radius varied from 17 to 336 cm^{-3}. Approximate calculations (using $Q(r) = 2$ and 0.75 μm mean radius) indicate that the highest concentration in the 0.75 - 1.25 μm range would reduce the visibility to around 1.3 km on its own and have an LWC around 10^{-3} gm^{-3}. If the droplets with $r > 1.25\mu m$ radius were associated with a visibility 430 m, this would be reduced to 360 m by the haze droplets.

Jiusto and Lala (1983) report concentrations between 0.25 and 1 μm radius of 195 - 288 cm^{-3}, with concentrations of larger drops in the range 54 - 197 cm^{-3}. These concentrations imply a similar contribution to the extinction coefficient to those of Kunkel estimated above. Jiusto and Lala also note that there were numerous haze droplets with $r < 0.25\mu m$ radius. In this size range Q(r)is decreasing to zero as r tends to zero, so they are likely to make only a small contribution to the extinction coefficient.

Mack et al. (1980) measured droplet concentrations with a Royco optical counter. The droplet concentration in the 0.15 - 1.5 μm radius range was 50 - 400 cm^{-3}, with most values less than 200 cm^{-3}. CCN concentrations at 0.2 % supersaturation varied from 40 to 680 cm^{-3} and so are much more compatible with the droplet concentration measurements than in Garland (1973). Using a TSI electrical aerosol analyser, concentrations of 5000 - 10000 cm^{-3} were obtained for $r > 0.005\mu m$. Assuming these are less than 0.15 μm radius, a small effect on the extinction coefficient is likely because of the decrease in Q(r).

One method of quantifying the effect of the haze droplets would be to make up drop-size distributions including haze droplets, then use equations (4), (5), and (10) to compute visibility and LWC. A simpler method has been adopted by modifying equation (11). Define a minimum radius r_m to be included in the fog drop range and used in the r_e calculation. LWC_r and r_e are the values calculated from drops with $r > r_m$. Define β_a, LWC_a as the extinction coefficient and LWC associated with the haze droplets, $r < r_m$. Then -

$$LWC_r = 4/3\pi\rho_l \int_{r_m}^{\infty} N(r) r^3 dr \quad \text{----------(12)}$$

$$r_e = \frac{\int_{r_m}^{\infty} N(r) r^3 dr}{\int_{r_m}^{\infty} N(r) r^2 dr} \quad \text{----------(13)}$$

$$V = \frac{3.0}{2\pi \int_{r_m}^{\infty} N(r) r^3 dr + \beta_a} \quad \text{----------(14)}$$

From (12) to (14) -

$$V = \frac{3.0 r_e}{3LWC_r / 2\rho_l + r_r \beta_a} \quad \text{----------(15)}$$

or

$$LWC_r = \frac{2 r_e \rho_l}{3} [\frac{3.0}{V} - \beta_a] \quad \text{----------(16)}$$

One can either produce a table of LWC_r against visibility for different r_e (i.e. corresponding to LWC from a drop-size distribution with a minimum radius) or use the total liquid water content LWC = $LWC_r + LWC_a$. The latter is used in Table 2.

LWC_a and β_a values have been calculated using as a basis a CCN distribution given in Hudson (1980). Most CCN spectra only go down to a supersaturation of 0.2%. An ammonium sulphate nucleus activated at 0.2% supersaturation has a droplet radius at 100% relative humidity of 0.2μm. Hudson presents CCN concentrations down to 0.04% supersaturation. An ammonium sulphate nucleus activated at this supersaturation has a radius of around 1μm at 100% relative humidity. The CCN spectrum is of the standard form, $N=CS^k$, where S is the supersaturation in %, N the concentration of CCN activated at S in cm^{-3}. Constants for a spectrum obtained in polluted San Diego air have been used to produce Table 2, C = 2500, k = 0.7. These constants produce a concentration of 451 cm^{-3} in the range $0.25 < r < 1.05$ μm, in good agreement with the measurements presented earlier. Hudson (1980) states that this CCN spectrum produces a visibility of 420 m at RH = 100%. However, at saturation, the largest nuclei have swollen to around 4 μm to produce such a visibility. Truncating the distribution at around 1 μm produces a visibility of 1917 m ($\beta_a = 1.545 \times 10^{-3}$ m^{-1}) and $LWC_a = 6.7 \times 10^{-4}$ gm^{-3} and these were used to produce Table 2. Supersaturation was converted to nucleus mass using a relationship for ammonium sulphate in Garland(1969). Nucleus mass was converted to radius at 100% relative humidity using -

$$r = \sqrt{\frac{Bm}{A}} \quad \text{----------(17)}$$

which follows from the simplified drop growth equation, e.g. Mason (1971), when dr/dt = 0 and RH = 100%. If r is in metres and nucleus mass m in Kg, $B = 6.05 \times 10^{-5}$ for an ammonium sulphate nucleus and $A = 1.15 \times 10^{-9}$. These constants produce radius values within a few percent of more rigorous calculations by Garland (1969).

Q(r) values for pure water were taken from Howell (1969) , assuming a wavelength of light of 0.55 μm.

3. Relationship Between LWC and Extinction Coefficient at Wavelengths of 8 - 13 μm

Chylek (1978) has shown that there is a linear relationship between LWC and the extinction coefficient in the 8 - 13 μm atmospheric window (β_{IR}). At these wavelengths, Q(r) ∝ r for drops up to about 14 μm radius. Assuming Q(r) = a.r where a is a constant appropriate to a given wavelength, Equation (5) gives

$$\beta_{IR} = a.\pi \int_0^\infty n(r).r^3 dr \quad \text{----------(18)}$$

Combining Equations (10) and (18) -

$$\beta_{IR} = \frac{3.a.LWC}{4.\rho_l} \quad \text{----------(19)}$$

The linear relationship between Q(r) and r breaks down for r > 14 μm but detailed calculations would be required to estimate the effect on the accuracy of Equation (19).

Appendix C. Details of Visibility and LWC Measurements Obtained from the Literature

Table 1C is a repeat of Table 5 but with an added indication of how the measurements were made. The method of measuring LWC and visibility is indicated as follows. LWC values obtained by integrating the over a measured drop-size distribution are indicated by a D. LWC can also be measured by drawing the foggy air into a container for a known time interval and capturing the fog droplets. The LWC is estimated by weighing the container before and after. Weighing techniques are indicated by a W. Visibility obtained from the drop size distribution is also labelled D, otherwise it is a direct measurement.

Only Wendisch et al. (1998) present r_e as a measure of drop size. When volume mean radius (r_v) is given r_e is estimated from $r_e = 1.1\ r_v$, (Liu and Hallett, 1997). Some of the references give r_v and arithmetic mean radius, r_a. This has enabled a typical value for r_v/r_a to be estimated and then used to convert r_a to r_v in references which only give the former. The ratio used is 1.4. A factor of 1.1 is then used to convert r_v to r_e.

Table 1C Summary of Fog Liquid Water Content Measurements Including Technique

Source	LWC (gm^{-3})	Visibility (m)	r_e (μm)
Garland et al. (1973)	0.04 - 0.22 (D & W)	230 - 42	-
Low (1975)	0.04 - 0.65 (D)	1000 - 84 (D)	9.2 - 18.5 (1.1 rv)
Pilie et al. (1975)	0.025 - 0.21 (W)	-	Up to 14 (1.1 rv)
Roach et al. (1976)	0.04 - 0.26 (D & W)	-	-
Pinnick et al. (1978)	Up to 0.4 aloft (D)	Min vis. 30 (D)	-
Brown (1980)	0.15 - 0.48 (D)	113 - 38 (D)	-
Mack et al. (1980)	0.023 - 0.21 at 5m 0.075 - 0.365 at 44m (D)	900 - 103 at 5m (D) 250 - 75 at 44m	7.5 - 15 at 5m 5.5 - 12 at 44m (from r_a)
Kunkel (1982)	0.047 - 0.24 case av. 0.02 - 0.52* point values (D)	453 - 68 case av. 1500 - 36 point values (D)	5.3 - 12.4 case av. 5.0 - 15 point values (D)
Dollard et al. (1983)	0.057 - 0.23	-	-
Jiusto et al. (1983)	0.03 - 0.50	814 - 75	3 - 7.3 (from r_a)
Wendisch et al. (1998)	0.092 - 0.31 case average (D)	-	5.8 - 11.0

* Corrected LWC values only go to 0.3 gm^{-3} but uncorrected values are given in Table 5 because only uncorrected visibilities are available.

Appendix D Ice Deposition Calculations

The collision efficiency of a drop (yet to be defined precisely) depends on the inertial parameter (K), Starr (1967).

$$K = \frac{\rho_l d^2 V}{9\eta D} \quad \text{----------(1)}$$

where ρ_l is the density of water, d drop radius, V airspeed, η viscosity of air and D object dimension. Physically, K is the ratio of the stopping distance of the drop when injected at velocity V into still air to the object dimension.

Calculations for a Cylinder

Object dimension D is taken as the cylinder diameter. The collision efficiency for the cylinder (E) was taken to be that which represents the fraction of flux of liquid water upwind of the cylinder which impinges on it. An expression for E due to Walton and Wallock (1960) has been used.

$$E = \frac{K^2}{(K+0.7)^2} \quad \text{----------(2)}$$

It has been checked that equation (2) agrees quite closely with plots of E vs. K (or K_0, to be defined later) presented in Starr (1967) and the FAA Aircraft Icing Handbook.

Per unit length of cylinder, the projected area normal to the airflow is equal to the diameter D and the rate at which mass is accreted is E.LWC.V.D. In order to convert this to a mean rate of depth of ice accretion one can divide by the half the area of the face of the cylinder i.e. $\pi D/2$. This assumes the cylinder is stationary so only half the area is facing upwind. For a rotating cylinder which becomes evenly coated one would divide by πD. Considering half the area -

$$\text{Rate of increase of depth deposited} = \frac{2.LWC.V.E.}{\pi\rho_i} \quad \text{----------(3)}$$

Calculations for an Aerofoil

The geometry of an aerofoil is obviously more complex than a cylinder and the theory and results given in the FAA Aircraft Icing Handbook (1991) have been used. The FAA Handbook gives graphs of collection efficiencies for various aerofoils as a function of adjusted inertia parameter K_0. Inertia Parameter K assumes the drag on the drop is given by Stokes Law whilst K_0 allows for deviations from this. K_0 was obtained from the following formula in the FAA Handbook -

$$K_0 = 18.K.[\mathrm{Re}^{-\frac{2}{3}} - \frac{\sqrt{6}}{\mathrm{Re}}.\arctan(\frac{\mathrm{Re}^{\frac{1}{3}}}{\sqrt{6}})] \quad \text{----------(4)}$$

where Re is the Reynolds Number of the drop -

$$\mathrm{Re} = \frac{\rho_a.V.d}{\eta} \quad \text{----------(5)}$$

While the FAA Handbook appears to calculate K from equation (1) for a cylinder, for an aerofoil

$$K = \frac{\rho_w . d^2 . V}{18\eta . c} \quad \text{----------(6)}$$

where c is the dimension of the chord of the aerofoil. A value of c of 3.2 ft (0.945 m) was used in producing Tables (7) to (9).

Two types of collection efficiency factor are presented in the FAA Handbook as functions of K_0. One of these is E, which has already been defined. The depth of deposition is very uneven for an aerofoil. Also, how far back from the leading edge deposition occurs depends on K_0 as well. Therefore, variations in E do not just reflect the thickness of ice accreted but the area over which accretion occurs. The FAA Handbook gives another parameter, the local impingement efficiency factor (β), which applies to a specific location. The FAA Handbook give graphs of the maximum value of β (β_{max}) against K_0 for various aerofoils and this parameter has been used to calculate the rates of deposition on an aerofoil in Tables (7) to (9). The maximum value of ice accretion rate (in mm h^{-1}) has been calculated because for the typical accretion rates expected under the various scenarios assumed the aerodynamic effect on the aerofoil is likely to be more significant than the weight of ice accreted.

Values of β_{max} were taken from Figure 2.51 of the FAA Handbook for a NACA 0012 aerofoil. For the lower windspeeds considered values of K_0 were less than 0.01 which is the lower limit of Figure 2.51. The β_{max} curve was virtually linear near $K_0 = 0.01$ and was extrapolated linearly to $\beta_{max} = 0$ at $K_0 = 3 \times 10^{-3}$. (The plot is of β_{max} vs $\log(K_0)$). Therefore, there is some uncertainty over the results for the 2 and 10 ms^{-1} wind speeds.

Figure 1a LWC vs Visibility - No Haze Droplets

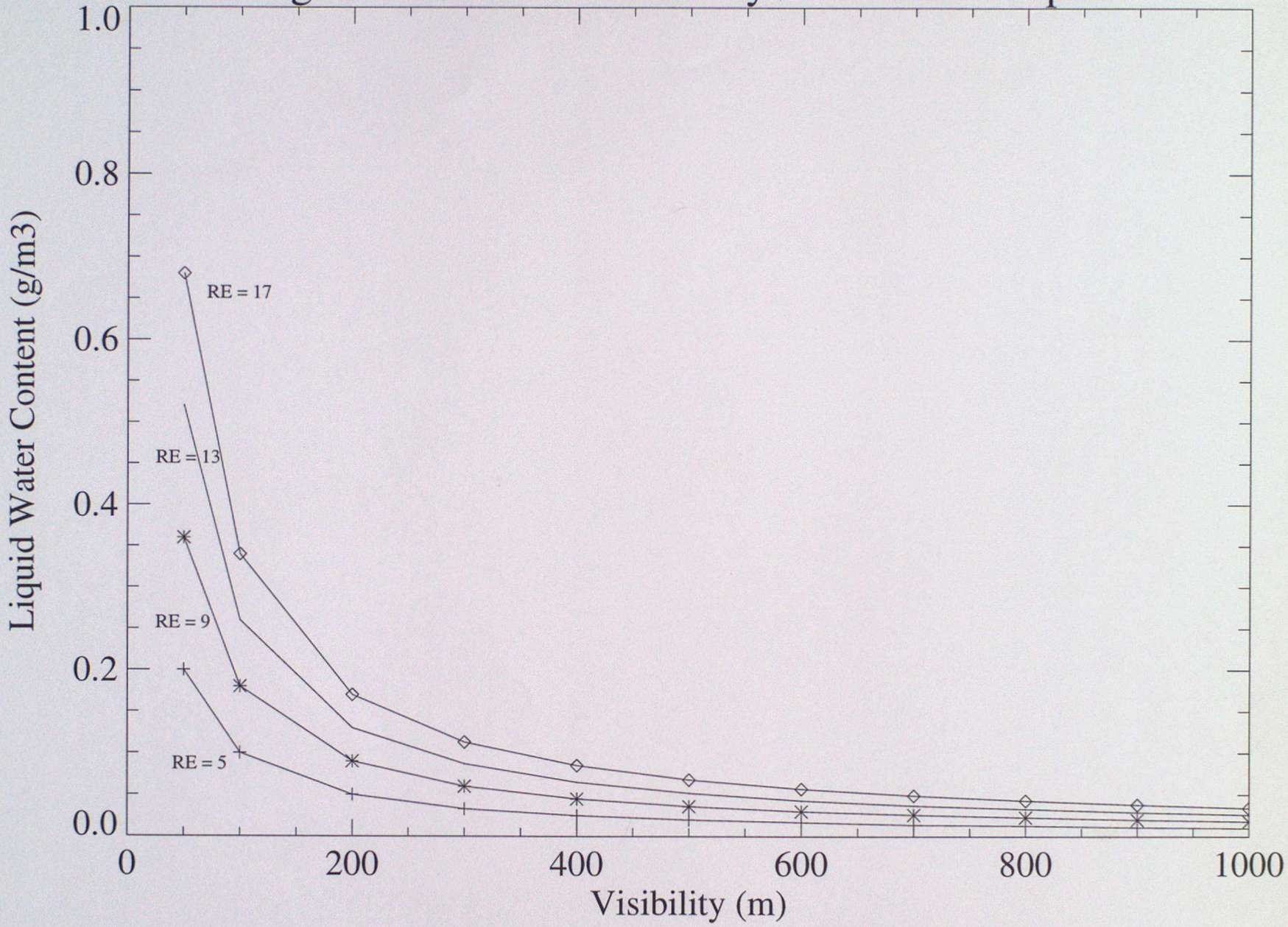

Figure 1b LWC vs Visibility - Including Haze Droplets

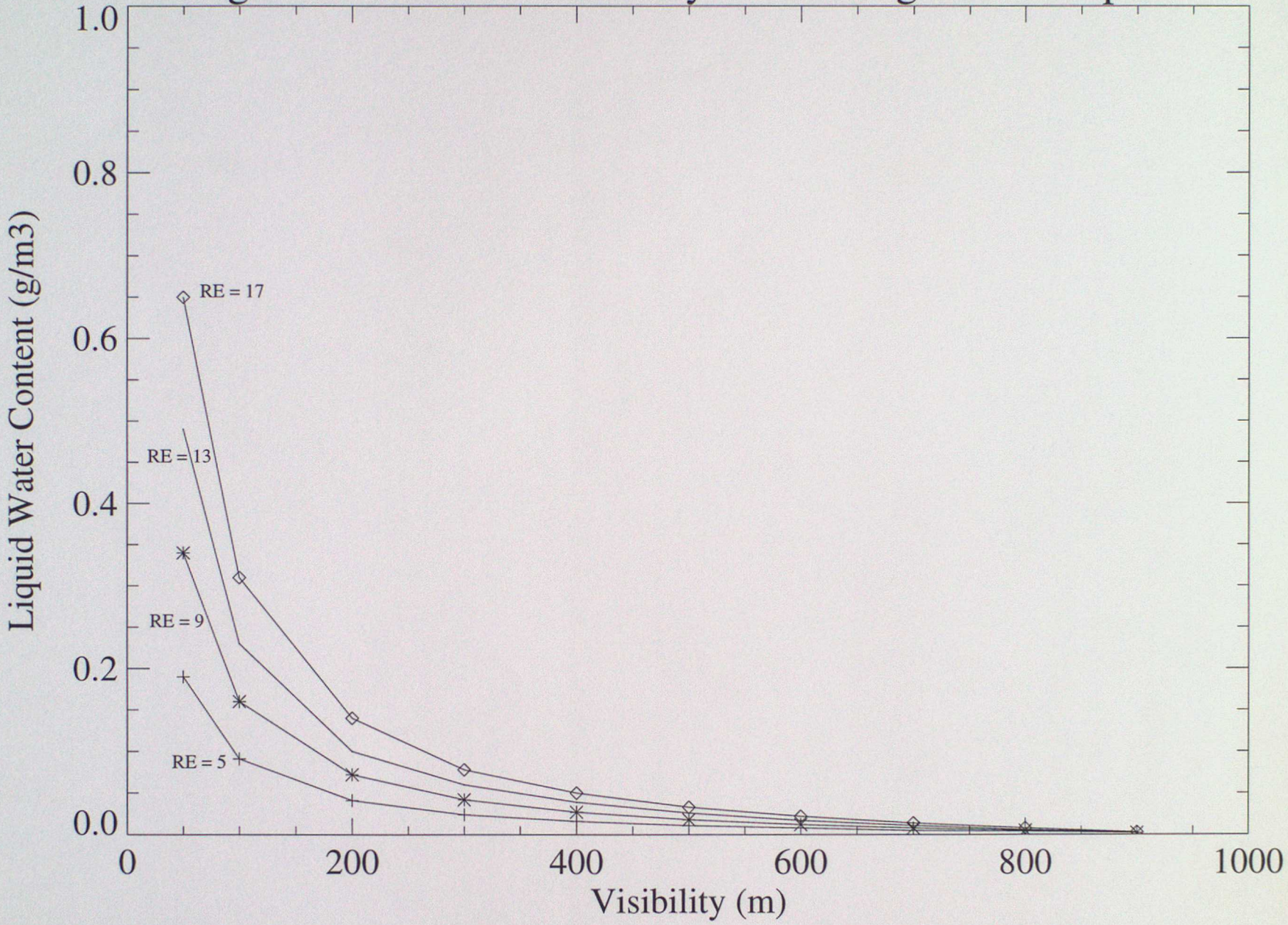

Figure 2 Observed visibility vs LWC

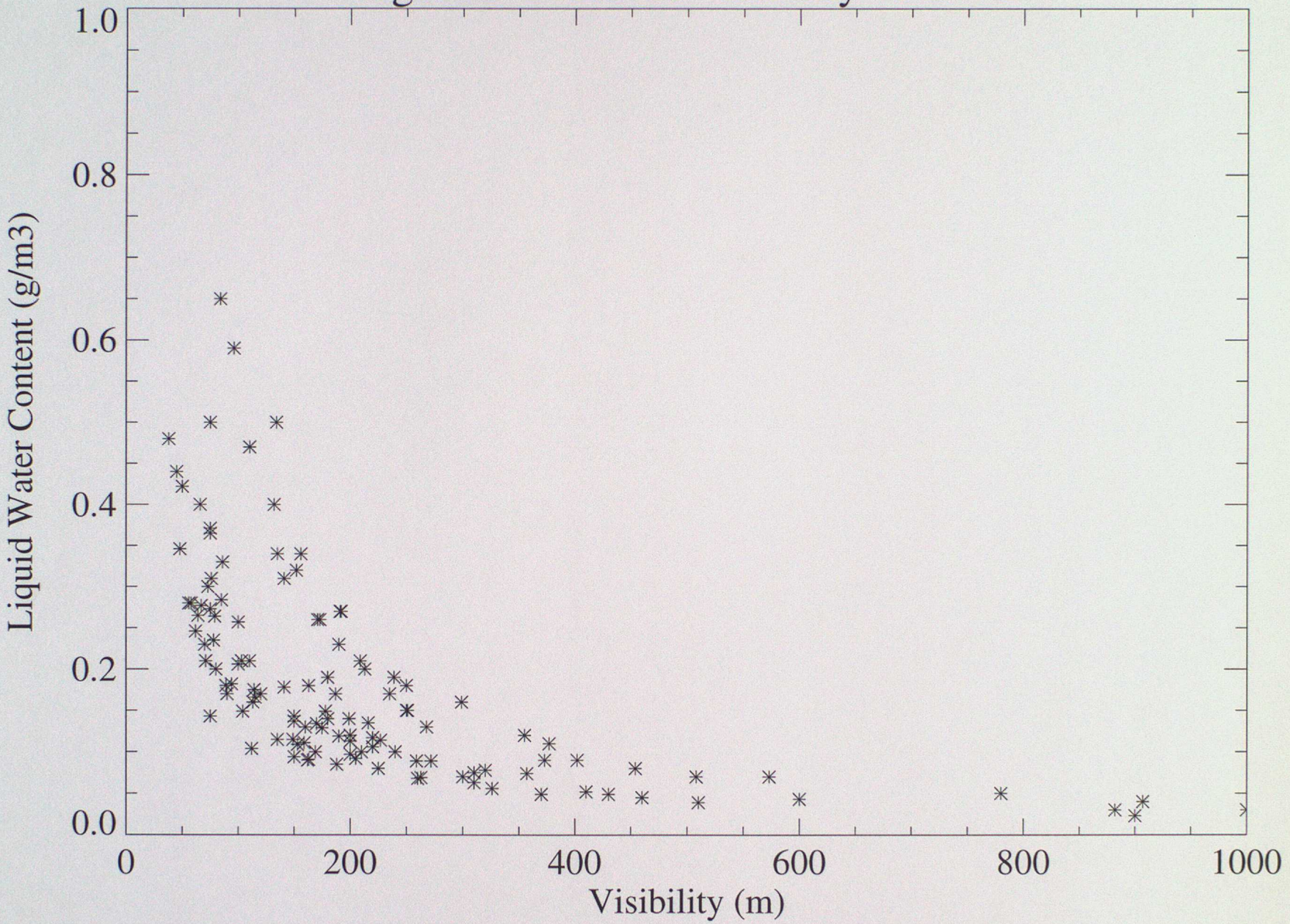

Figure 3a Deposition Rate Assuming E = 1 (mm/h)

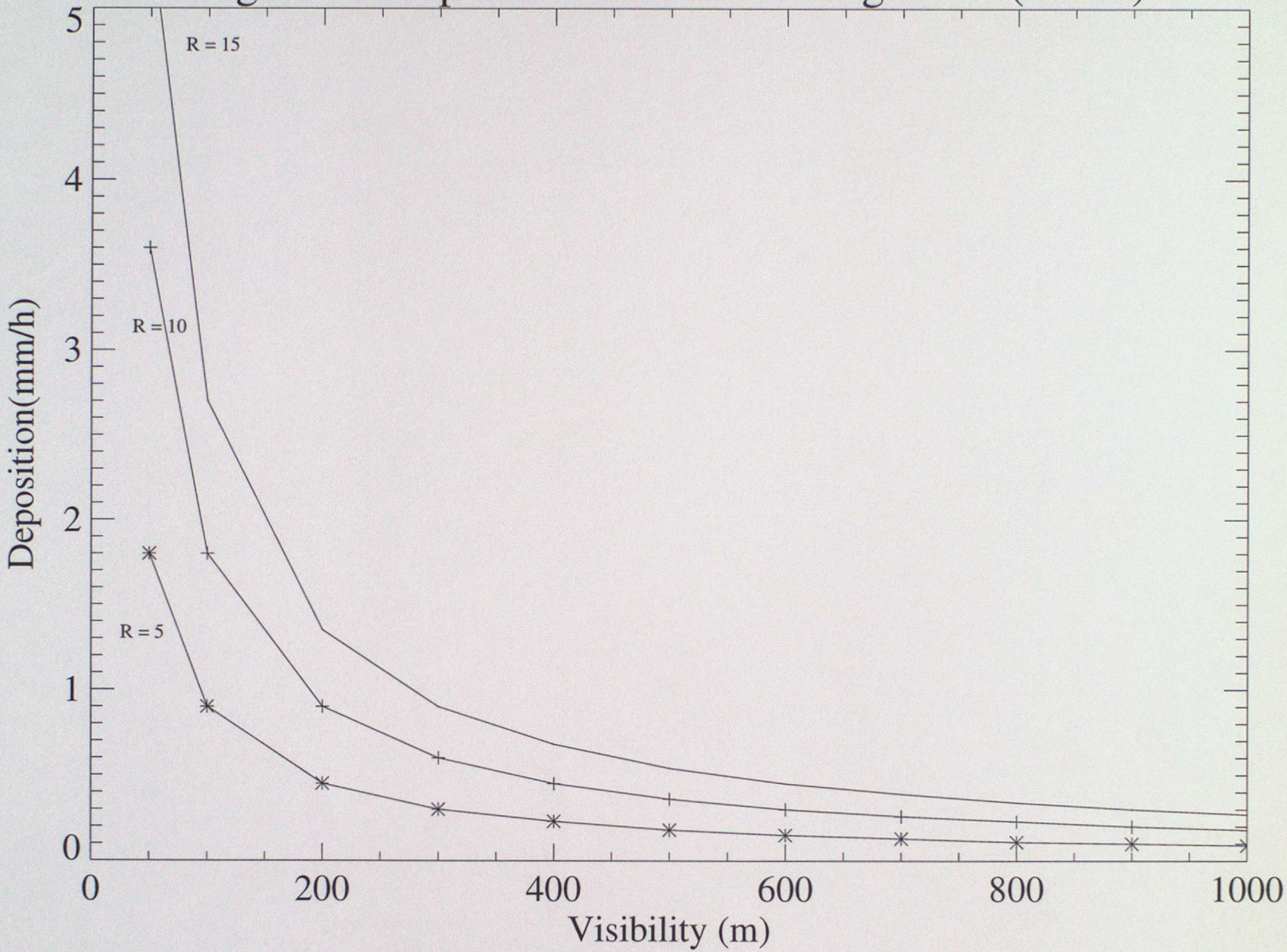

Figure 3b Deposition Rate on 1 cm Diam. Cylinder (mm/h)